ANALYSIS OF TURBULENCE MODELS AND INVESTIGATION OF THE STRUCTURE OF THE FLOW IN A HYDROCYCLONE

O. V. Matvienko   UDC 621.928.37

A numerical investigation of the structure of the flow in a hydrocyclone has been carried out on the basis of Reynolds equations with the use of various models of turbulence: the k–ε model, the k–ε RNG (ReNormaliza-tion Group) model, the k–ε model corrected for the Richardson number Ri, and the k–ω model. It is shown that the distributions of the velocities and pressure in a hydrocyclone obtained with the k–ε Ri model, in which the influence of the rotation of the flow on the processes of generation/dissipation of turbulence and the anisotropy of the turbulent pulsations are taken into account, coincide most closely with the experimental ones.

Apparatus of the hydrocyclone type are widely used in the mineral resource and ore mining and processing industries for the purpose of separation and classification of inhomogeneous disperse systems. The widespread use of these apparatus is explained, in many cases, by their simple design, fairly high capacity compared to their small dimensions, relatively low cost, and low expenses required for their exploitation.

The present work is a continuation of the investigations begun at the Erlangen University (Germany) with financial support from the Alexander von Humboldt Foundation [1–5].

It has been shown earlier that the structure and separation characteristics of the flow in a hydrocyclone are mainly determined by the flow turbulence. Thus, it is desired to find a turbulence model that would make it possible to predict the distribution of the velocities and pressure in a hydrocyclone most adequately.

The aim of the present work is to investigate the structure of the flow in a hydrocyclone and perform a comparative analysis of four turbulence models: the standard k–ε model [6], the k–ε RNG model [7], the k–ε model corrected for the Richardson number Ri [8], and the k–ω model [9]. This task was a considerable challenge because of the nonlinearity of the basic equations (Reynolds equations) and the complex geometry of the computational region. Since three-dimensional effects appear only in a relatively small region near the inlet pipe and the flow in the main body of the hydrocyclone is almost axially symmetric [10], the changes in the parameters in the tangential direction can be ignored to simplify the mathematical model and the calculations.

Mathematical Model. The flow field is described using the two-dimensional axisymmetric Reynolds equations of mass and momentum balance for an average flow:

$$\frac{\partial \rho u}{\partial x} + \frac{1}{r}\frac{\partial \rho vr}{\partial r} = 0 , \tag{1}$$

$$\frac{\partial \rho u^2}{\partial x} + \frac{1}{r}\frac{\partial \rho uvr}{\partial r} = -\frac{\partial p}{\partial x} + \frac{\partial}{\partial x}\left[\mu_e\left(2\frac{\partial u}{\partial x} - \frac{2}{3}\left(\frac{\partial u}{\partial x} + \frac{1}{r}\frac{\partial vr}{\partial r}\right)\right)\right] + \frac{1}{r}\frac{\partial}{\partial r}\left[\mu_e r\left(\frac{\partial u}{\partial r} + \frac{\partial v}{\partial x}\right)\right], \tag{2}$$

$$\frac{\partial \rho uv}{\partial x} + \frac{1}{r}\frac{\partial \rho v^2 r}{\partial r} = -\frac{\partial p}{\partial r} + \frac{\partial}{\partial x}\left[\mu_e\left(\frac{\partial v}{\partial x} + \frac{\partial u}{\partial r}\right)\right] + \frac{1}{r}\frac{\partial}{\partial r}\left[\mu_e r\left(2\frac{\partial v}{\partial r} - \frac{2}{3}\left(\frac{\partial u}{\partial x} + \frac{1}{r}\frac{\partial vr}{\partial r}\right)\right)\right] - 2\frac{\mu_e v}{r^2} + \frac{\rho w^2}{r} , \tag{3}$$

$$\frac{\partial \rho u w}{\partial x} + \frac{1}{r}\frac{\partial \rho v w r}{\partial r} = \frac{\partial}{\partial x}\left[\mu_e \frac{\partial w}{\partial x}\right] + \frac{1}{r^2}\frac{\partial}{\partial r}\left[\frac{\mu_e}{\sigma_{r\varphi}} r^3 \frac{\partial}{\partial r}\left(\frac{w}{r}\right)\right] - \frac{\rho v w}{r}\,. \tag{4}$$

The main problem of modeling of turbulence is associated with the determination of the Reynolds stresses. This problem is most often solved based on the Boussinesq hypothesis. In accordance with this hypothesis, the Reynolds stresses are linearly related to the average-velocity gradient and, as the proportionality coefficient, the coefficient of turbulent viscosity μ_t, defined as $\mu_t = C_\mu \rho k^2 \varepsilon^{-1}$, is used [6]. The effective viscosity is determined as the sum of the molecular and turbulent viscosity, $\mu_e = \mu_0 + \mu_t$.

The kinetic turbulent energy k and the rate of its dissipation ε can be determined using the standard k–ε model of turbulence from the following equations:

$$\frac{\partial \rho u k}{\partial x} + \frac{1}{r}\frac{\partial \rho v k r}{\partial r} = \frac{\partial}{\partial x}\left[\frac{\mu_e}{\sigma_k}\frac{\partial k}{\partial x}\right] + \frac{1}{r}\frac{\partial}{\partial r}\left[\frac{\mu_e}{\sigma_k} r \frac{\partial k}{\partial r}\right] + G_k - \rho\varepsilon\,, \tag{5}$$

$$\frac{\partial \rho u \varepsilon}{\partial x} + \frac{1}{r}\frac{\partial \rho v \varepsilon r}{\partial r} = \frac{\partial}{\partial x}\left[\frac{\mu_e}{\sigma_\varepsilon}\frac{\partial \varepsilon}{\partial x}\right] + \frac{1}{r}\frac{\partial}{\partial r}\left[\frac{\mu_e}{\sigma_\varepsilon} r \frac{\partial \varepsilon}{\partial r}\right] + (C_1 - C_2 \rho\varepsilon)\frac{\varepsilon}{k}\,, \tag{6}$$

$$G_k = \mu_t \left\{ 2\left[\left(\frac{\partial u}{\partial r}\right)^2 + \left(\frac{\partial v}{\partial r}\right)^2 + \left(\frac{v}{r}\right)^2\right] + \left(\frac{\partial u}{\partial r} + \frac{\partial v}{\partial x}\right)^2 + \left(\frac{\partial w}{\partial x}\right)^2 + \left(r\frac{\partial w/r}{\partial r}\right)^2 \right\}. \tag{7}$$

The values of the constants are selected in accordance with the recommendations of [4]: $C_1 = 1.44$, $C_2 = 1.92$, $C_\mu = 0.09$, $\sigma_k = 1.0$, $\sigma_\varepsilon = 1.3$, and $\sigma_{r\varphi} = 1.0$.

The k–ε RNG model of turbulence [7] is a modification of the standard k–ε model and differs from it by the values of the constants: $C_1 = 1.42 - C_{1RNG}$, $C_2 = 1.68$, $C_\mu = 0.085$, $\sigma_k = 0.7179$, $\sigma_\varepsilon = 0.7179$, $\sigma_{r\varphi} = 1.0$, $C_{1RNG} = \dfrac{\eta(\eta_0 - \eta)}{\eta_0(1 + \beta\eta^3)}$, $\eta_0 = 4.38$, $\beta = 0.015$, and $\eta = \sqrt{C_k/\mu_t}\,\dfrac{k}{\varepsilon}$.

The k–ε model corrected for the Richardson number Ri [8] has been obtained in the following way. It was assumed that the turbulent viscosity in the equations for axial motion $\mu_{rx} = \mu_e$ and rotational motion $\mu_{r\varphi} = \mu_e / \sigma_{r\varphi}$ ($\sigma_{r\varphi} = 2.5$) is nonisotropic, and the constant C_2 in Eq. (6) was corrected with the use of the Richardson number Ri $= \dfrac{k}{\varepsilon^2}\dfrac{w^2}{r}\dfrac{\partial(wr)}{\partial r}$ for the purpose of more exact description of the influence of the swirling of the flow on the processes of generation/dissipation of turbulence. The values of the constants and the functions in this model are as follows: $C_1 = 1.44$, $C_2 = 1.92(1 - C_3 Ri)$, $C_\mu = 0.09$, $\sigma_k = 1.0$, $\sigma_\varepsilon = 1.3$, and $C_3 = 0.001$.

The k–ε model of turbulence [9] can be used as an alterative to various modifications of the k–ε model. In it, the frequency of the turbulent pulsations $\omega = \varepsilon/k$ is used as the second parameter characterizing the distribution of turbulence in the flow.

The equations used in this model are similar to the equations of the k–ε model:

$$\frac{\partial \rho u k}{\partial x} + \frac{1}{r}\frac{\partial \rho v k r}{\partial r} = \frac{\partial}{\partial x}\left[\frac{\mu_e}{\sigma_k}\frac{\partial k}{\partial x}\right] + \frac{1}{r}\frac{\partial}{\partial r}\left[\frac{\mu_e}{\sigma_k} r \frac{\partial k}{\partial r}\right] + G_k - \rho\omega k\,, \tag{8}$$

$$\frac{\partial \rho u \omega}{\partial x} + \frac{1}{r}\frac{\partial \rho v \omega r}{\partial r} = \frac{\partial}{\partial x}\left[\frac{\mu_e}{\sigma_\omega}\frac{\partial \omega}{\partial x}\right] + \frac{1}{r}\frac{\partial}{\partial r}\left[\frac{\mu_e}{\sigma_\omega} r \frac{\partial \omega}{\partial r}\right] + (C_1 k^{-1} - C_2 \rho\omega)\,\omega\,, \tag{9}$$

$$\mu_t = C_\mu \rho k \omega^{-1}\,. \tag{10}$$

The constants of the model have the following values: $C_1 = 0.5111$, $C_2 = 0.8333$, $C_\mu = 0.09$, $\sigma_k = 2$, $\sigma_\omega = 2$, and $\sigma_{r\varphi} = 1$.

Since the system of differential equations is elliptical, to close the problem it is necessary to set conditions at all the boundaries of the computational region.

The conditions at the inlet (in the inlet pipe) are determined for all the variables. To ensure that the problem be two-dimensional, it is assumed that the inlet of the hydrocyclone represents a cylindrical surface the height of which is equal to the diameter of the inlet pipe. The kinetic turbulent energy at the inlet is taken to be proportional to the kinetic energy of the average flow. Thus, the boundary conditions at the inlet are formulated in the following way:

$$v = \frac{Q}{\pi D_c D_{in} \rho}, \quad u = \frac{\alpha Q}{\pi D_c D_{in} \rho}, \quad w = \frac{Q}{h_{in} D_{in} \rho}, \quad k = Tu w_{in}^2, \quad \varepsilon = 2\frac{k_{in}^{3/2}}{\lambda D_c}.$$

Here, $\alpha = 0.15$, $\lambda = 0.005$, and $Tu = 0.03$ are constants of the model.

At the symmetry axis, the radial components of the gradients of all the functions, excluding the radial and tangential velocities that are equal to zero here, are assumed to be zero:

$$v = 0, \quad \frac{\partial u}{\partial r} = 0, \quad w = 0, \quad \frac{\partial k}{\partial r} = 0, \quad \frac{\partial \varepsilon}{\partial r} = 0.$$

The adhesion conditions are fulfilled at the walls of the hydrocyclone and all the velocity components tangential to the hydrocyclone walls are equal to zero. The derivative of the velocity with respect to the normal to the wall is also equal to zero. The turbulent characteristics are determined on the assumption that a local equilibrium exists in the near-wall region:

$$v = 0, \quad u = 0, \quad w = 0, \quad k_{nw} = \frac{\tau_w}{\rho \sqrt{C_\mu}}, \quad \varepsilon_{nw} = \frac{k_{nw}^{3/2} C_\mu^{3/4}}{\kappa r_{nw}}.$$

Here, $k = 0.4$ and r_{nw} is the distance from the hydrocyclone wall to the nearest near-wall node.

At the output of the hydrocyclone (in both the overflow and the underflow) the axial components of the tangential-velocity gradient and of the turbulent characteristics k and ε are assumed to be zero in order that the influence of the counterflow be excluded. It is assumed that the radial velocity v in the output cross sections is equal to zero. The pressure p in the overflow is determined on the assumption that the flow is radially equilibrium, whereas the pressure in the underflow is assumed to be equal to the atmospheric pressure. Thus, the boundary conditions in the output cross sections can be as follows:

$$\frac{\partial p}{\partial r} = \frac{\rho w^2}{r} \text{ (overflow)}, \quad p = p_{env} \text{ (underflow)}, \quad v = 0, \quad \frac{\partial w}{\partial x} = 0, \quad \frac{\partial k}{\partial x} = 0, \quad \frac{\partial \varepsilon}{\partial x} = 0.$$

The above-described mathematical model is based on the system of Reynolds equations in dynamic variables. A finite-difference analog of the system of differential equations has been obtained by integrating them over the control volume of a finite-difference grid. The calculations were performed with the use of biased grids with 100 nodes in the radial direction and 300 nodes in the axial direction. The convective terms were approximated using upwind differences by the QUICK scheme. The diffusion terms were modeled with the use of an exponential approximation. Because of the nonlinearity of the system of finite-difference equations, it was solved by the iteration method with a longitudinal-transverse run in each iteration. The pressure was calculated using the SIMPLE iteration procedure [11].

Results of the Calculations. Based on the above-described mathematical model, we have carried out a numerical investigation of the structure of the flow in a hydrocyclone (Fig. 1). The calculation parameters of the apparatus had values corresponding to the experiments in [10]: $D_c = 75$ mm, $D_{in} = 25$ mm, $D_{of} = 25$ mm, $D_{uf} = 12.5$ mm, $L_1 = 75$ mm, $L_2 = 200$ mm, $L_3 = 25$ mm, $l_1 = 50$ mm, $l_2 = 50$ mm, and $h_{in} = 4$ mm.
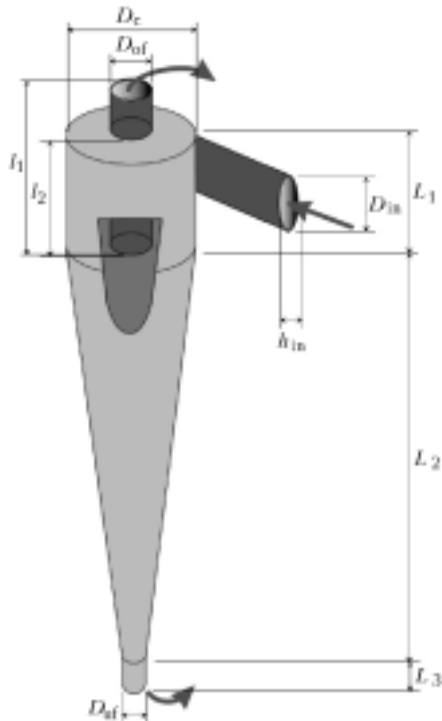
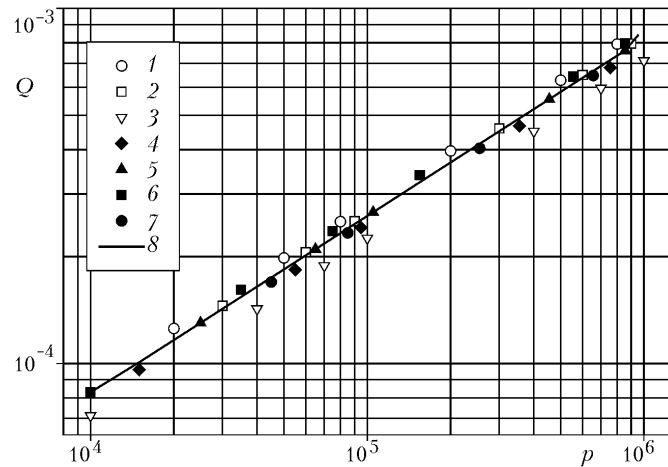Fig. 1. External view and diagram of a hydrocyclone.

Fig. 2. Capacity of the hydrocyclone (m^3/sec): 1–3) experimental data of [14] (1), [15] (2), and [16] (3); 4–7) calculation data obtained with the k–ε Ri model (4), the standard k–ε model (5), the k–ε RNG model (6), and the k–ω model (7); 8) average value of the calculation data.

Below we give the most interesting results. From the engineering standpoint, the most important parameters characterizing the structure of the flow in a hydrocyclone are its capacity and the distribution of flows in it.

The capacity of a hydrocyclone Q characterizes the amount of a suspension which can be processed by it in a unit time. From the hydraulics standpoint, a hydrocyclone can be considered as a hydraulic resistance in an inlet pipe. Its capacity depends on the head loss, which is determined, first of all, by the dimensions of the discharge openings. To pass a required amount of a suspension though a hydrocyclone and obtain the desired technological parameters, it is necessary to create a pressure immediately ahead of the inlet pipe which would be able to overcome the hydraulic resistance in it and the centrifugal pressure arising as a result of the flow rotation. In this case, the major portion of the head losses are due to the centrifugal pressure. The head losses caused by the hydraulic resistance at the inlet do not usually exceed 20%.

In the technical literature there are a large number of formulas for calculating the capacity of hydrocyclones. Some of them are given in monographs [12, 13]. Some literature data and the data of our calculations are presented in Fig. 2. It is seen from the figure that the computational points constructed in logarithmic coordinates with the use of different models of turbulence are practically coincident and lie on a straight line. The experimental points are grouped around the calculated straight line, which sufficiently well predicts the hydrocyclone capacity. The latter increases with increase in the total head. In this case, the slope of the straight line calculated in logarithmic coordinates is equal to 1/2 and the hydrocyclone capacity is proportional to the square root of the total head.

The ratio between the liquid-flow rates in the overflow and the underflow is a major preoccupation of the study of the hydrocyclone operation. If it were possible to develop a method of exactly determining the distribution of liquid volumes between the overflow and the underflow of a hydrocyclone by the given initial parameters, this would make the calculation of the other parameters much simpler.

The distribution of liquid volumes between the overflow and the underflow (split) $S = Q_{uf}/Q_{in}$ is determined first of all by the ratio between the diameters of the discharge openings D_{uf}/D_{of}. However, at a constant discharge
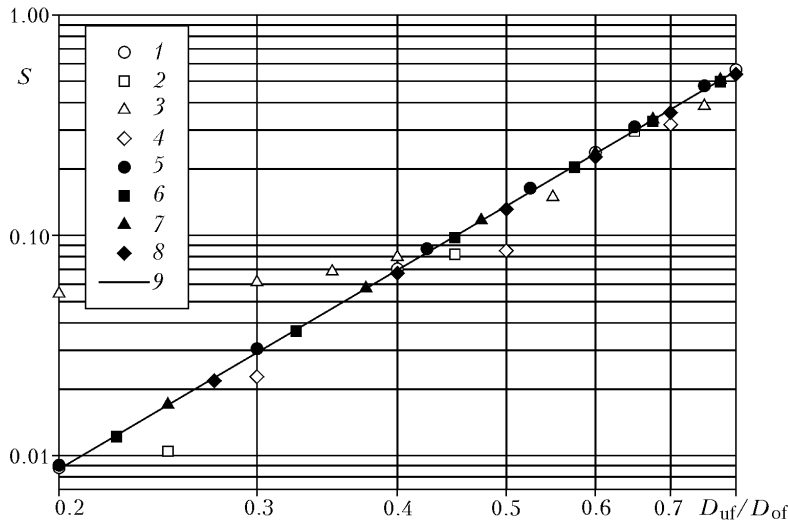
Fig. 3. Distribution of the liquid flow rate between the overflow and the underflow versus the ratio between the diameters of the discharge openings: 1–4) experimental data of [13] (1), [13] (2), [17] (3), and [18] (4); 5–8) calculation data obtained with the k–ε Ri model (5), the standard k–ε model (6), the k–ε RNG model (7), and the k–ω model (8); 9) average value of the calculation data.
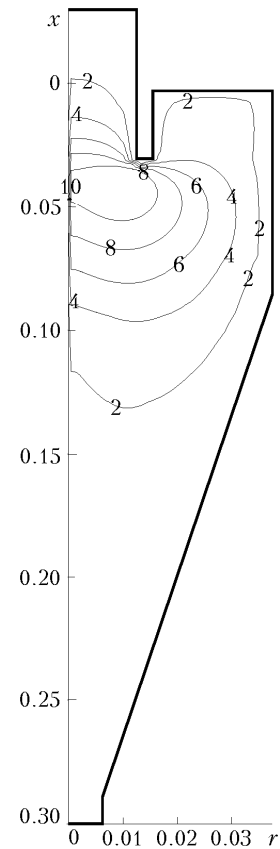
Fig. 4. Isolines of kinetic turbulent energy in the hydrocyclone (k–ε Ri model), m^2/sec^2.

ratio, the split of a hydrocyclone depends on a number of conditions, among which are the granulometric composition and the weight content of the solid phase in the suspension, the pressure at the inlet, and the geometric parameters and design of the hydrocyclone.

In the majority of cases, the hydrocyclone split was investigated for hydrocyclones of small dimensions operating on water. Some results of such investigations are presented in Fig. 3. As is seen from the figure, all of the above-described four models of turbulence give practically the same result. It is also seen that the experimental data agree closely with the calculation data, except for the data of [17], which, evidently, have been obtained for a hydrocyclone working on a suspension.

In addition to the integral parameters, it is also interesting to consider the distributions of the turbulence, velocity, and pressure characteristics in a hydrocyclone.

It is important to know the turbulence characteristics of a hydrocyclone, because the structure of the flow and the motion of particles in it are substantially dependent on the flow turbulence. Unfortunately, the turbulence in a hydrocyclone was not experimentally investigated. This is explained by the fact that it is difficult to measure pulsating velocities. Therefore, only the theoretical analysis can make up for this deficiency.

Figure 4 shows isolines of kinetic turbulent energy in a hydrocyclone. It is seen from the figure that the kinetic turbulent energy has highest values at the lower edge of the vortex tube where the flow turns and the velocity gradients are very large. Then, because of the convection, turbulence is carried to the lower part of the hydrocyclone
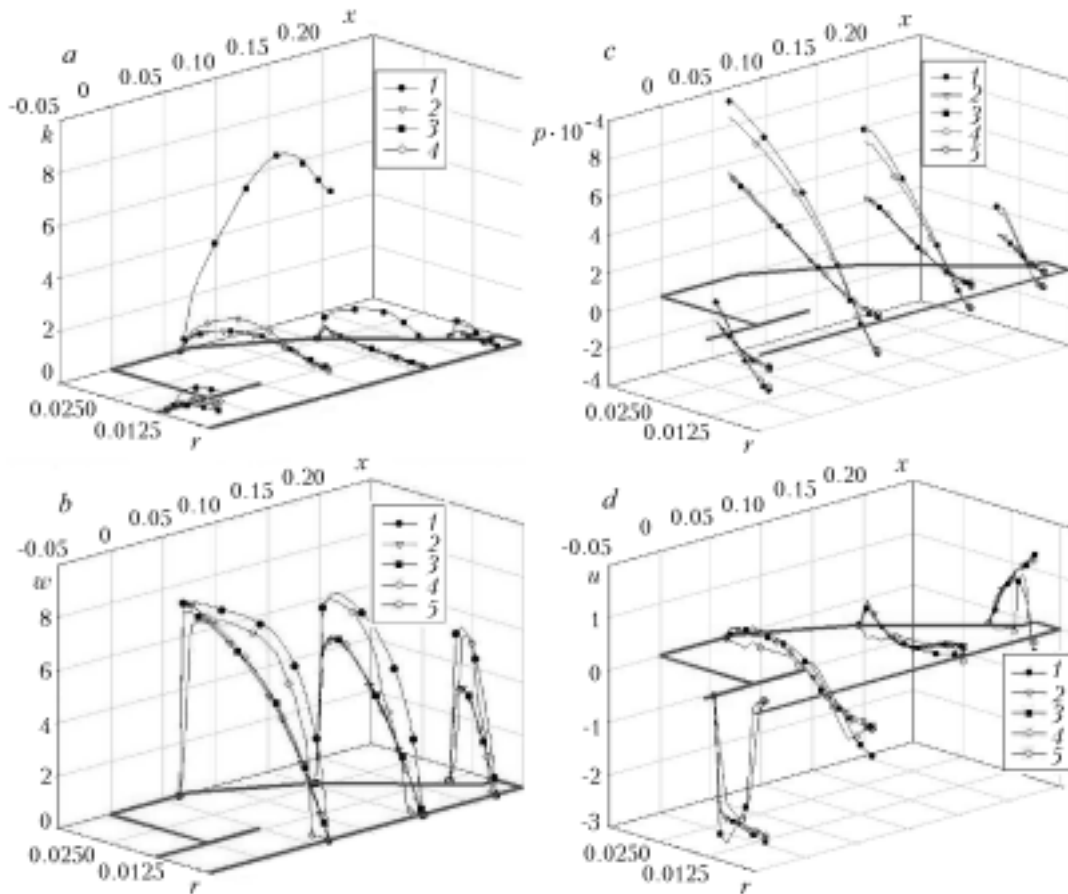
Fig. 5. Radial distribution of the characteristic of the flow in the hydrocyclone:
1) k–ε Ri model; 2) standard k–ε model; 3) k–ε RNG model; 4) k–ω model;
5) experimental data; a) kinetic turbulent energy; b) tangential velocity; c)
pressure; d) axial velocity.

and gradually decays. It is interesting to note that the increase in the kinetic turbulent energy in the neighborhood of the underflow is due to the inflow of free air to the central part of the underflow and the formation of an air column.

The isolines in Fig. 4 have been constructed using the k–ε model of turbulence. The other models of turbulence give qualitatively the same turbulent-energy distributions. The quantitative differences between them can be judged from Fig. 5a, in which radial turbulent-energy distributions calculated with the use of different models of turbulence are shown. As is seen from this figure, the kinetic turbulent-energy distributions calculated with the standard k–ε model, the k–ε RNG model, and the k–ω model are practically the same (analogous results have been obtained for the pressure distribution and the distributions of the axial and tangential velocities). At the same time, the k–ε Ri model gives higher values of the kinetic turbulent energy. This can be explained by the fact that, in it, the influence of swirling of the flow on the processes of turbulent-energy generation/dissipation is taken into account. It is known [19] that the centrifugal forces arising in swirling flows can be active, conservative, or indifferent with respect to the action on the flow turbulization. The Richardson number can be used as a characteristic of such an action.

The centrifugal forces cause an additional turbulization of the flow in the channel at Ri > 0, aid the relaminarization of the flow at Ri < 0, and have no influence on the flow at Ri = 0.

An analysis of the radial distribution of the tangential velocity (Fig. 5b) has shown that at the core of the flow this velocity increases smoothly from zero at the flow axis to any maximum value in the peripheral part of the flow, and then w decreases because of the adhesion to the wall. It should be noted that, at the core of the flow, the radial distribution of the tangential velocity can be modeled by the dependence $w = ar^n$, where a and n are any positive constants. Thus, Ri > 0 at the core of the flow. This explains the higher values of the kinetic turbulent energy obtained with the use of the k–ε Ri model.

The tangential velocity in the conic part of the hydrocyclone increases with decrease in the radius of the flow rotation and can exceed the velocity of the inflow at the interface between the outer and inner flows. The calculations have shown that the tangential velocity increases with increase in the pressure at the inlet and with decrease in the diameter of the discharge opening.

The k–ε Ri model gives higher tangential velocities than other models of turbulence, which is explained by the fact that it takes into account the anisotropy of the swirling turbulent flow which manifests itself as a decrease in the viscous-stress-tensor component $\mu_{e\varphi}$ by a factor of 2.5. The experimental distributions of the tangential velocity obtained in [10] lie between the distributions predicted by the k–ε Ri model and the other models. In this case, the data obtained with the k–ε Ri model of turbulence agree most closely with the experimental data.

Figure 5c shows a radial distribution of the pressure in the hydrocyclone in the four different cross sections. The pressure in the near-axis region is close to the atmospheric pressure. In this case, the calculation of the pressure with the use of the standard k–ε model, the k–ε RNG model, and the k–ω model has shown that the pressure in the near-axis region is higher than the atmospheric pressure. The data obtained with the k–ε Ri model point to a rarefaction in the near-axis region: the pressure in this region is lower than the atmospheric pressure, which correlates well with the experimental data [20]. When one (or both) discharge openings are opened, air is drawn in to this zone, with the result that an air column is formed. Thus, the k–ε Ri model of turbulence makes it possible to calculate the formation of an air column in a hydrocyclone. The pressure in the peripheral region increases sharply and reaches the maximum value in the neighborhood of the wall. The pressure changes insignificantly in the axial direction as compared to the changes in it in the radial direction; this being so, the isobars are practically parallel to the hydrocyclone axis.

Figure 5d shows experimental and calculated distributions of the axial velocity in the four cross sections of the hydrocyclone. The axial velocities in all the horizontal cross sections positioned lower than the outlet pipe increase in the direction from the hydrocyclone wall to the near-axis zone. The velocity values change from the positive to negative, passing though zero at the center of the hydrocyclone radius. In the region positioned higher than the outlet pipe, near its wall, the axial velocities decrease. Thus, there exists a conical surface, on which the axial velocity of the flow is zero. The liquid inside this surface moves up, and the liquid outside it moves to the underflow. The absolute velocity of the external flow is lower than that of the internal flow. Approximately at the center of the conical part of the hydrocyclone, the liquid moves from the external flow to the internal flow, with the result that the velocity of the latter increases.

The calculations performed with the use of the standard k–ε model, the k–ε RNG model, and the k–ω model have shown that liquid flows out of the hydrocyclone with no ejection of air from outside, but this is in contradiction with the experimental data. A more real pattern has been obtained with the use of the k–ε Ri model of turbulence in which the turbulent viscosity is assumed to be nonisotropic and the constant C_2 in the equation for ε is corrected for the Richardson number. It is seen from Fig. 5d that the k–ε Ri model of turbulence gives a more real pattern of the flow. At the output of the hydrocyclone (in both the overflow and the underflow) a certain amount of air enters the apparatus. Even though these features of the flow are close to those observed in experiments, the internal structure of the flow differs substantially from the real one. For example, the calculated dimensions of the air-circulation zones in the neighborhood of the overflow and the underflow are substantially smaller than the experimental ones.

Thus, the turbulence models used at present for calculating hydrocyclones need further improvements. Nonetheless, our analysis shows that the k–ε Ri model of turbulence can be used for calculating the characteristics of the flow in a hydrocyclone.

NOTATION

C_1, C_{1RNG}, C_2, C_μ, C_3, parameters of the turbulence model; D_c, diameter of the hydrocyclone, mm; D_{in}, diameter of the inlet pipe, mm; D_{of}, diameter of the outlet pipe, mm; D_{uf}, diameter of the underflow, mm; G_k, dissipation function, J/(m^3·sec); h_{in}, width of the inlet pipe, mm; k, kinetic turbulent energy, J/kg; L_1, length of the cylindrical section, mm; L_2, length of the conical section, mm; L_3, length of the post-cyclone, mm; l_1, total length of

the outlet pipe, mm; l_2, length of the outlet-pipe part positioned deeper in the hydrocyclone, mm; Q, mass flow rate, kg/sec; p, pressure, Pa; r, radial coordinate, m; S, distribution of liquid volumes between the overflow and the underflow; u, axial velocity, m/sec; v, radial velocity, m/sec; w, tangential velocity, m/sec; x, axial coordinate, m; ε, rate of turbulent-energy dissipation, J/(kg·sec); μ_0, dynamic molecular viscosity, kg/(m·sec); μ_e, effective viscosity, kg/(m·sec); μ_t, turbulent viscosity, kg/(m·sec); k, Kármán constant; ρ, density, kg/m^3; σ_k, σ_ε, $\sigma_{r\varphi}$, parameters of the turbulence model; τ_w, stresses on the wall, kg/(m·sec^2); ω, frequency of turbulent pulsations, sec^{-1}; Ri, Richardson number; Tu, turbulence parameter. Subscripts; c, cyclone; env, environment; e, effective; in, input; nw, near-wall; of, overflow; t, turbulent; uf, underflow; w, wall.

REFERENCES

1. O. Matvienko, J. Dück, and Th. Neeβe, Numerische Simulation der Strömungen in einem Hydrozyklon, in: *Book of Abstracts of the Annual Meeting "Gesellschaft fur Angewandte Mathematik und Mechanik*," Bremen, April 6–9 (1998), p. 85.

2. O. Matvienko, J. Dück, and Th. Neeβe, A mathematical simulation of hydrocyclone hydrodynamics, in: M. Sommerfeld (ed.), *Proc. 9th Workshop on Two-Phase Flow Predictions*, Merseburg (1999), pp. 194–202.

3. O. Matvienko, J. Dück, and Th. Neeβe, Hydrodynamics and particle separation in the hydrocyclone, in: *Proc. 2nd Int. Symp. on Two-Phase Flow Predictions and Experimentation*, Pisa, Italy, May 23–26, 1999, Pisa (1999), pp. 923–928.

4. J. Dück, O. V. Matvienko, and Th. Neeβe, Modeling of hydrodynamics and separation in a hydrocyclone, *Teor. Osn. Khim. Tekhnol.*, **34**, No. 5, 478–488 (2000).

5. J. Dueck, O. Matvienko, and Th. Neeβe, Numerical modelling of hydrocyclone dynamics for process control, in: *Proc. 14th Annual Techn. Conf. and Exposition "Science and Technology of Filtration and Separation for the 21th Century,"* Tampa, Florida, May 1–4, 2001, pp. 153–167.

6. B. E. Launder and D. B. Spalding, The numerical computation of turbulent flows, *Comput. Meth. Appl. Mech. Eng.*, **3**, 269–289 (1974).

7. V. Yakhot and S. A. Orszag, Renormalization group analysis of turbulence. I. Basic theory, *J. Sci. Comput.*, **1**, 1–51 (1986).

8. F. Boysan, Numerical modelling of cyclone separation, *Selected Topics in Two-Phase Flow*, *Lectures Series*, **9**, 137–158, Trondheim, Norway (1984).

9. D. C. Wilcox, Reassessment of the scale-determining equation for advanced turbulence models, *AIAA J.*, **26**, No. 11, 1299–1310 (1988).

10. T. C. Monredon, K. T. Hsien, and R. K. Rajamani, Fluid flow model of the hydrocyclone: An investigation of device dimensions, *Int. J. Mineral Process.*, **35**, 65–83 (1992).

11. S. Patankar, *Numerical Heat Transfer and Fluid Flow* [Russian translation], Énergoatomizdat, Moscow (1984).

12. L. Svarovsky, Hydrocyclones, London (1984).

13. A. I. Povarov, *Hydrocyclones at Concentrating Mills* [in Russian], Nedra, Moscow (1978).

14. F. J. Fontein, Wirkung des Hydrozyklons und des bogensiebs sowiederen Anwendungen, *Aufbereitungs Technik*, No. 3, S. 85–89 (1961).

15. H. Trawinski, Der Hydrozyklon als Hilfsgerät zur Grundstoffveredelung, *Cheme-Ing. Techn.*, **25**, No. 6, 331–340 (1953).

16. A. N. Izmailova, *Study of Hydrocyclone Operation on Suspensions of Polymers*, Candidate Dissertation (in Engineering), Leningrad (1969).

17. N. Joshioka and J. Hotta, Liquid cyclone as hydraulic classifier, *Chem. Eng. Japan*, **19**, 632–635 (1955).

18. G. Tarjan, Bewegungsvorgange im Hydrozyklon und seine Anwendung in der Schwerstubeaufbereitung, *Neue Hutte*, **4**, No. 2, 65–74 (1959).

19. V. K. Shchukin and A. A. Khalatov, *Heat Transfer, Mass Transfer, and Hydrodynamics of Swirling Flows in Axisymmetric Channels* [in Russian], Mashinostroenie, Moscow (1982).

20. D. F. Kellsal, A further study of the hydraulic cyclone, *Chem. Eng. Sci.*, **30**, 254–272 (1953).